Second-order susceptibility in asymmetric quantum wells and its control by proton bombardment

S. J. B. Yoo, M. M. Fejer, and R. L. Byer
Edward L. Ginzton Laboratory, Stanford University, Stanford, California 94305

J. S. Harris, Jr.
Stanford Electronics Laboratory, Stanford University, Stanford, California 94305

(Received 17 December 1990; accepted for publication 15 February 1991)

We report measurements of extremely large mid-infrared second-order susceptibilities due to intersubband transitions in an asymmetric quantum well, and selective suppression of these susceptibilities by proton bombardment of the sample. The measured second-order susceptibility for second-harmonic generation of 9.25–10.78 μm is in good agreement with theoretical calculations based on measured infrared absorption spectra, which show the lowest two intersubband transitions. The peak value of the susceptibility is 58 nm/V, 320 times larger than the bulk nonlinear susceptibility of GaAs.

Intersubband transitions in quantum wells have extremely large oscillator strengths and relatively narrow linewidths,[1] suggesting a variety of applications, including nonlinear optical frequency conversion.[2–6] Previous experiments have found susceptibilities for second-harmonic generation (SHG) as large as 28 nm/V in quantum wells under a bias electric field[7] and as large as 760 nm/V in asymmetric wells.[8] A large nonlinear susceptibility alone is inadequate for efficient nonlinear devices; means for phase matching are also necessary. An attractive technique for overcoming phase velocity dispersion, quasi-phase-matching, involves periodic modulation of the nonlinear susceptibility.[9,10] In this letter we describe measurements of the infrared absorption of asymmetric quantum wells,[11,12] which show the allowed and the normally disallowed transitions, and measurements of the dispersion of the nonlinear susceptibility, which show resonances at these transition energies. We also demonstrate spatial modulation of the magnitude of the susceptibilities through proton bombardment.

Figure 1 shows a diagram of the asymmetric quantum well and the subband wave functions. The sample, grown on a semi-insulating GaAs substrate by molecular beam epitaxy in a Varian Gen-II system, consists of a 1 μm GaAs layer doped at $n = 10^{18}$ cm^{-3}, a 500 Å buffer region of undoped $Al_{0.55}Ga_{0.45}As$, 50-periods of the quantum well structure, another 500 Å buffer region of undoped $Al_{0.55}Ga_{0.45}As$, and a 0.5 μm GaAs layer doped at $n = 10^{18}$ cm^{-3}. The barriers of the quantum well structure consist of 80 Å undoped $Al_{0.55}Ga_{0.45}As$, 10 Å GaAs doped at $n = 3\times10^{18}$ cm^{-3}, 100 Å undoped $Al_{0.55}Ga_{0.45}As$, 10 Å GaAs doped at $n = 3\times10^{18}$ cm^{-3}, and 80 Å undoped $Al_{0.55}Ga_{0.45}As$. The wells are undoped, and consist of 60 Å $Al_{0.21}Ga_{0.79}As$ and 35 Å GaAs. The dopant in all cases is silicon. Thin GaAs layers are used for doping in the AlGaAs barrier to minimize *DX* center formation.[13]

Knowledge of the intersubband transition energies and dipole matrix elements is necessary to model the optical properties of the quantum well structure. We obtain the envelope functions, ψ_n, in the effective mass approximation by solving $H\psi_n = E_n\psi_n$, where E_n is the energy eigenvalue. We take the effective mass Hamiltonian to be

$$H(z) = -\frac{\hbar}{2}\frac{d}{dz}\frac{1}{m^*(z)}\frac{d}{dz} + U(z), \tag{1}$$

where $\hat{z}$ is normal to the layers. The dependence of the conduction-band potential $U(z)$ and effective mass $m^*(z)$ on composition is taken from Ref. 14, and nonparabolicity is accommodated in the calculation by defining an energy-dependent effective mass $m^*(E)$[15] according to $h^2k^2/2m^*(E) = E(k)$, where $E(k)$ is the dispersion relation given in Ref. 16. Solving Eq. (1) numerically, we find the dipole matrix elements $\langle z_{ij}\rangle = \langle\psi_i|z|\psi_j\rangle$, and transition energies $\hbar\Omega_{ij} = (E_i - E_j)$ shown in Table I, including first-order corrections for band bending. The oscillator strengths, given by $f_{ij} = 2m_e\Omega_{ij}\langle z_{ij}\rangle^2/\hbar$ under the assumption of unity overlap of the Bloch functions, and the integrated absorption fraction (IAF), calculated according to Eq. (5) of Ref. 1, are also shown in this table. Note the large oscillator strength of the 1–3 transition, which is forbidden in symmetric structures.

Figure 2 shows a single pass Brewster angle absorption spectrum measured at room temperature with a Digilab

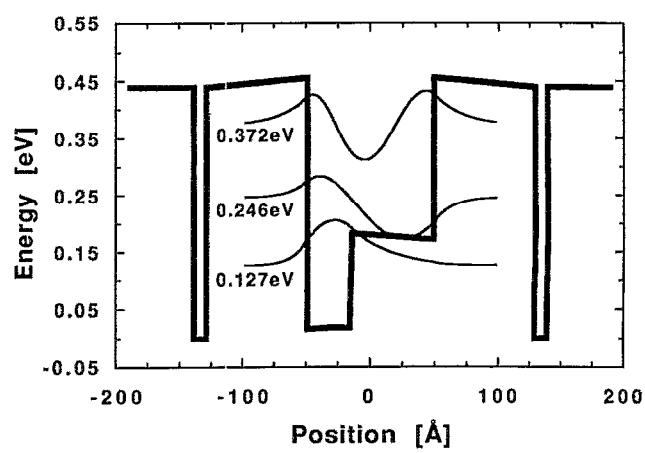

FIG. 1. Diagram of the quantum well structure and subband wave functions. The theoretical energy levels and potential energies including first-order corrections for band bending are shown.

 0003-6951/91/161724-03$02.00

TABLE I. Theoretical energy, dipole matrix elements, and absorption strengths between the subbands in the quantum well.

Transition level	Energy (meV)	Dipole matrix element (Å)	Oscillator strength	IAF (Abs cm^{-1})
1–2	119.5	− 14.5	6.61	2.24
1–3	245.9	− 7.9	4.03	1.34
2–3	126.4	− 23.0	17.6	0.06
1–1	···	− 23.8	···	···
2–2	···	16.9	···	···
3–3	···	− 3.4	···	···

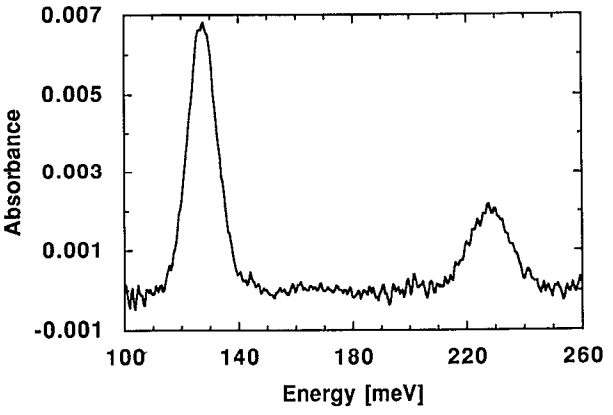

FIG. 2. Absorption spectrum measured at Brewster's angle. Absorption features at 127.6 and 228.2 meV correspond to the 1–2 transition and the 1–3 transitions, respectively.

FTS40 Fourier transform infrared spectrometer. The 1–2 and the 1–3 transitions are measured at 127.6 meV with full width at half maximum (FWHM) of 11.6 meV and at 228.2 meV with FWHM of 16.6 meV, respectively. These transition energies differ by 8.1 and − 17.7 meV, respectively, with the theoretical values of E_{21} and E_{31} in Table I, and the IAFs are smaller by factors of 2.24 and 3.05, respectively. Since the agreement of the experimental and the theoretical values of the transition energies, especially for E_{21}, is good, and that of the ratio $\mathrm{IAF}_{21}/\mathrm{IAF}_{31}$ is reasonable, we proceed in the remainder of this letter with the assumption that the error in the IAF_{21} is due to an effective carrier density being smaller than the dopant density. We calculate an effective sheet charge density $N_{\mathrm{eff}} = 2.64\times 10^{11}$ cm^{-2} by forcing agreement between the theoretical and the experimental values of the IAF_{21}. With this assumption, we find that the experimental IAF_{31} corresponds to $|z_{31}| = 7.2$ Å, 9% smaller than the theoretical value. The depolarization shifts[17] are a few meV, so that the 17.7 meV error in E_{31} is probably due to neglect of many-body effects, the approximate treatment of nonparabolicity, or deviations of the structure from the design values.

The nonlinear polarizability for second-harmonic generations is given by[18]

$$\alpha^{(2)}_{zzz}=\frac{2e^3}{\epsilon_0\hbar^2}\sum_{mn}\langle z_{1n}\rangle\langle z_{nm}\rangle\langle z_{m1}\rangle\{[(\omega-\Omega_{n1}-i\gamma_{n1})(2\omega-\Omega_{m1}-i\gamma_{m1})]^{-1}+[(\omega+\Omega_{n1}-i\gamma_{n1})(2\omega+\Omega_{m1}-i\gamma_{m1})]^{-1}-(2\omega-\Omega_{mm}-i\gamma_{mn})^{-1}[(\omega-\Omega_{m1}-i\gamma_{m1})^{-1}+(\omega+\Omega_{n1}-i\gamma_{n1})^{-1}]\}, \quad (2)$$

where we have assumed only the ground state is populated, e is the magnitude of the electronic charge, and $1/\gamma_{ij}$ is the dephasing time. In the low density limit, $\chi^{(2)}\cong N_{\mathrm{eff}}\alpha^{(2)}/L$, where L is the period of the structure. The solid line in Fig. 3 is calculated in this limit, using Eq. (2) with the effective carrier density, the empirical values of $\langle z_{31}\rangle$, γ_{21}, γ_{31}, and the theoretical values for the other parameters.

Experimental values of $\chi^{(2)}$ were obtained from second-harmonic generation measurements using a grating tuned, Q-switched CO_2 laser. The laser output was typically a train of 200 ns pulses with a peak power of 0.5 kW at a 100 Hz repetition rate, and was focused to a 50-μm-diam spot on the sample. The generated second harmonic was detected by a photovoltaic InSb detector behind a sapphire filter. To extract the absolute value of $\chi^{(2)}_{\mathrm{QW}}$, the second-harmonic power generated in the quantum well sample was normalized to that generated in a 108-μm-thick undoped GaAs plate in the same apparatus, using $\chi^{(2)}_{\mathrm{GaAs}} = 1.80\times 10^{-10}$ m/V.[19]

The total second-harmonic output is the coherent sum of the contributions from the quantum well intersubband states and the bulk GaAs substrate. For a fundamental beam polarized in the plane of incidence, propagating at an angle θ with respect to $\hat{z}$ inside the sample, and polarized in the plane of incidence, the total second-harmonic power is given by

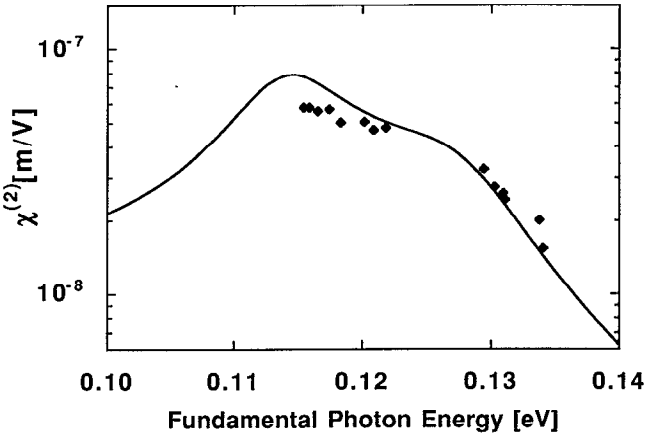

FIG. 3. Theoretical (line) and measured (diamonds) nonlinear susceptibilities due to intersubband transitions in the quantum wells.

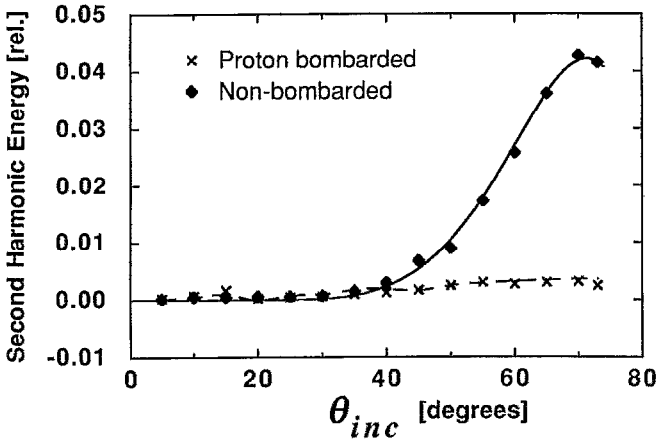

FIG. 4. Generated second-harmonic pulse energy as a function of angle of incidence on the quantum well sample (θ_{inc}), normalized to the output of the reference sample at Brewster's angle. Results for proton bombarded regions are indicated by crosses and for nonbombarded regions by diamonds. The latter set of data points are curve fit according to Eq. (3). Broken line shows data for a blank substrate.

$$P_{2\omega} \propto P_{\omega}^2 \left| t_{\omega}(\theta)^2 t'_{2\omega}(\theta) [\chi^{(2)}_{QW} \sin^3\theta + A(\theta)\chi^{(2)}_{GaAs} \sin\theta \cos^2\theta \sin 2\varphi] \right|^2. \quad (3)$$

Here, $t_{\omega}(\theta)$ and $t'_{2\omega}(\theta)$ are the transmission coefficients from air to GaAs for the fundamental and from GaAs to air for the second harmonic, respectively, $A(\theta)$ is a complex phase matching dependent factor, φ is the angle between a [100] axis of the crystal and the intersection of the plane of the incidence with the surface of the wafer, and $\chi^{(2)}_{QW}$ and $\chi^{(2)}_{GaAs}$ are the nonlinear susceptibilities of the quantum well structure and bulk GaAs, respectively. Measurements of $P_{2\omega}$ vs φ for Brewster angle incidence ($\theta_{inc} = 73°$) and $P_{2\omega}$ vs θ_{inc} for $\varphi = 0$ for a range of wavelengths are in good agreement with this expression, where θ_{inc} is the angle of incidence. Figure 4 shows the second-harmonic pulse energy vs θ_{inc} for a sample with asymmetric quantum wells (shown as diamonds) and a fit according to Eq. (3) (solid line). For comparison, data for a blank substrate are shown as a broken line.

The measured $\chi^{(2)}_{QW}$ at 9.25–10.78 μm is plotted in Fig. 3. The agreement between theory and experiment is reasonable in view of the uncertainty in the device and material parameters, and the neglect of many-body effects. The largest value of $\chi^{(2)}_{QW}$, measured at a fundamental wavelength of 10.78 μm, is 58 nm/V, 320 times larger than the nonlinear susceptibility of bulk GaAs.

Control of the $\chi^{(2)}_{QW}$ is important for device applications where phase matching is necessary. In Ref. 7, control of the sign and magnitude of $\chi^{(2)}_{QW}$ through an applied electric field was demonstrated. For many device applications, it would be more convenient to pattern $\chi^{(2)}_{QW}$ without resort to applied fields. Here, proton bombardment is used to eliminate the carriers and thus reduce $\chi^{(2)}_{QW}$. To test this technique, we remove the 0.5 μm cap layer by wet etching, and then exposed the sample to six steps of room-temperature proton bombardment. The proton energies and doses were chosen to create a trap density at least three times the carrier density throughout the structure.[20] After proton bombardment, an absorption measurement showed no resolvable intersubband absorption (less than 5% of the absorption of the undamaged region). The results of a second-harmonic generation measurement in the proton bombarded region are shown as the crosses in Fig. 4. The measured second-harmonic pulse energies are indistinguishable from those for the blank substrate, indicating that, to the resolution of the measurement, the proton bombardment eliminated the nonlinear susceptibility due to intersubband transitions in the quantum wells.

In conclusion, we report measurement of the linear and the second-order susceptibilities due to intersubband transitions in a compositionally asymmetric quantum well. The linear absorption measurement shows both the 1–2 transition and the 1–3 transition as expected. The resonant energies and relative absorption strengths of the transitions agree well with theoretical predictions. The measured $\chi^{(2)}_{QW}$ in the CO_2 laser tuning range is also in good agreement with theory. The largest $\chi^{(2)}_{QW}$ measured is 58 nm/V. Proton bombardment was used to pattern the magnitude of the susceptibilities, a technique which can be used for periodic modulation of $\chi^{(2)}_{QW}$ to achieve quasi-phase-matching in a waveguide structure.

The authors would like to thank T. Ma for growing of the sample, and acknowledge NSF grant DMR 87-21735 and JSEP N00014-84-K-0327 for financial support.

[1] L. C. West and S. J. Eglash, Appl. Phys. Lett. **46**, 1156 (1985).
[2] M. K. Gurnick and T. A. DeTemple, IEEE J. Quantum Electron. **19**, 791 (1983).
[3] S. J. B. Yoo, M. M. Fejer, Alex Harwit, R. L. Byer, and J. S. Harris, Jr., J. Opt. Soc. Am. A **4**, P27 (1987).
[4] L. Tsang, D. Ahn, and S. L. Chuang, Appl. Phys. Lett. **52**, 697 (1988).
[5] E. Rosencher, P. Bois, J. Nagel, E. Costard, and S. Delaitre, Appl. Phys. Lett. **55**, 1597 (1989).
[6] J. Khurgin, J. Opt. Soc. Am. B **6**, 1673 (1989).
[7] M. M. Fejer, S. J. B. Yoo, R. L. Byer, Alex Harwit, and J. S. Harris, Jr., Phys. Rev. Lett. **62**, 1041 (1989).
[8] E. Rosencher, P. Bois, J. Nagle, and S. Delaitre, Electron. Lett. **25**, 1063 (1989).
[9] J. A. Armstrong, N. Eloembergen, J. Ducuing, and P. S. Pershan, Phys. Rev. **127**, 1918 (1962).
[10] Sasson Somekh and Amnon Yariv, Opt. Commun. **6**, 301 (1972).
[11] Janet L. Pan, Lawrence C. West, Susan J. Walker, Roger J. Malik, and John F. Walker, Appl. Phys. Lett. **57**, 366 (1990).
[12] Y. J. Mii, K. L. Wang, R. P. G. Karunasiri, and P. F. Yuh, Appl. Phys. Lett. **56**, 1046 (1990).
[13] P. M. Mooney, T. N Theis, and S. L. Wright, Appl. Phys. Lett. **53**, 2546 (1988).
[14] S. Adachi, J. Appl. Phys. **58**, R1 (1985).
[15] Gerald Bastard, *Wave Mechanics Applied to Semiconductor Heterostructures* (Les Éditions de Physique, Les Ulis Cedex, France, 1988), Chap. 2.
[16] J. S. Blakemore, J. Appl. Phys. **53**, R 123 (1982).
[17] S. J. Allen, Jr., D. C. Tsui, and B. Vinter, Solid State Commun. **20**, 425 (1976).
[18] Y. R. Shen, *The Principles of Nonlinear Optics* (Wiley, New York, 1984), Chap. 2.
[19] B. F. Levine and C. G. Bethea, Appl. Phys. Lett. **20**, 272 (1972).
[20] J. F. Gibbons, W. S. Johnson, S. W. Mylroie, *Projected Range Statistics*, Semiconductors and Related Materials, 2nd ed. (Dowden, Hutchinson & Ross, Inc., Stroudsberg, 1975).